Composites Part B 132 (2018) 188–196

Contents lists available at ScienceDirect

Composites Part B

journal homepage: www.elsevier.com/locate/compositesb

Morphology controllable microwave absorption property of polyvinylbutyral (PVB)-MnO_2 nanocomposites

Pritom J. Bora [a], Irthasa Azeem [b], K.J. Vinoy [c], Praveen C. Ramamurthy [a, b, *], Giridhar Madras [a]

[a] Interdisciplinary Centre for Energy Research (ICER), India
[b] Department of Materials Engineering, India
[c] Department of Electrical and Communication Engineering, Indian Institute of Science, Bangalore 560012, India

ARTICLE INFO

Article history:
Received 7 May 2017
Received in revised form
6 September 2017
Accepted 7 September 2017
Available online 8 September 2017

ABSTRACT

This work reports the synthesis of polyvinylbutyral (PVB)-MnO_2 nanocomposites and their microwave absorption property. Anisotropic nanoparticles loaded polymer nanocomposites have better dielectric properties. Therefore, to investigate the morphology controlled microwave absorption property, MnO_2 nanorods and MnO_2 nanospheres were synthesized by low temperature chemical precipitation method and PVB-MnO_2 nanocomposites were solution processed. The microwave absorption of PVB was enhanced by MnO_2 nanorods compared to MnO_2 nanospheres, for both X-band (8.2–12.4 GHz) and Ku-band (12.4–18 GHz). The lowest reflection loss (RL) of PVB-MnO_2 nanorod composites was found to be -37 dB with a large bandwidth at the thickness of 2 mm while PVB-MnO_2 nanosphere composites show almost a linear decrease of RL with a minimum value −10 dB. It was observed that the enhancement of electromagnetic attenuation constant (α) and dielectric loss is the major factor responsible for the enhanced microwave absorption of PVB-MnO_2 nanorod composite. Further, morphology controls the microwave absorption property of PVB-MnO_2 nanocomposites through effective permittivity, degree of EM impedance matching (Δ), antenna mechanism, and dielectric dissipation that enhances high loss factor (LF %). The obtained high LF (84%) of PVB-MnO_2 nanorod composite indicates the excellent microwave absorption property and can be treated as a novel coating polymer nanocomposite for microwave absorption based applications.

1. Introduction

Microwave absorbing materials (MAM) have gained importance owing to their effectiveness in reducing the problem of electromagnetic interference (EMI), caused by the escalation of wireless communication systems, digital systems and electrical appliances [1–5]. MAMs have also gained attention because of their potential to be used in various applications such as in the aerospace and defence industry for stealth technology purposes, which utilizes the EM waves in the GHz frequency range [2,6]. MAMs can dissipate microwaves and are classified into three groups, namely electric loss medium, magnetic loss medium and dielectric loss medium based on their attenuation mechanism [1–5]. The absorption properties of an absorber strongly depend on its complex relative permeability (μ_r), permittivity (ε_r), electromagnetic impedance match, microstructure and the frequency of operation (f) [1,4,6]. A diverse range of materials such as carbonaceous materials [7–9], magnetic materials (ferrites) [8,10–12], conducting polymers [13,14], graphene based materials [12,16] have been studied and proven to exhibit microwave absorption. The graphitized reduced graphene oxide (rGO) is the thinnest and lightest material in the carbon family and has excellent electromagnetic interference (EMI) shielding efficiency [9].

Considerable research efforts have been made towards the development of novel microwave absorbing materials because the conventional materials cannot satisfy all of the requirements such as light weight, wide bandwidth, low thickness, ease of fabrication, environmental adaptability and superior microwave absorption properties [3,4]. From the recent studies, polymer matrices incorporated with appropriate fillers were found to be satisfying the

* Corresponding author. Interdisciplinary Centre for Energy Research (ICER), India.
E-mail address: onegroupb203@gmail.com (P.C. Ramamurthy).

http://dx.doi.org/10.1016/j.compositesb.2017.09.014
1359-8368/

aforementioned requirements along with other physical and mechanical properties such as low density, specific strength and corrosion resistance [2,12,15,24]. Juan et al. studied the microwave absorption of RGO/$MnFe_2O_4$/PVDF composites and observed a reflection loss (RL) of - 29 dB at 9.2 GHz for a filler loading of 5 wt% at a thickness of 3 mm [12]. The microwave absorption properties nano-structured metal oxides such as ZnO, SnO_2, NiO, CoOx and MnOx have been extensively studied [16–20]. Among these materials, manganese oxide (MnO_2) has advantages such as different crystal structure, good dielectric properties, low cost, good thermal stability, ease of production and is naturally abundant [15]. It has also been used to synthesize conducting polymer/conducting polymer nanocomposites [21,22]. Yan et al. studied the microwave absorption properties of MnO_2 hollow microspheres that consisted of MnO_2 nanoribbons synthesized by a hydrothermal method and reported RL of - 40 dB at 14.2 GHz (4 mm) [23]. Zhou et al. reported a facile hydrothermal synthesis technique for three different types of hollow urchin like α-MnO_2 nanostructures with good microwave absorbing properties [24]. Cheng et al. studied the microwave absorption of 3D sponge-like porous networks of manganese oxide nanoparticles and reported RL of −27.1 dB at 3.1 GHz for Mn_3O_4 nanoparticles [16]. Lv et al. reported −15 dB RL at 12 GHz for rod-like β-MnO_2-Fe-graphene nanocomposite with paraffin wax (1:1) at a thickness of 3 mm [25]. Similarly, the minimum RL value of −30 dB (11 GHz) was reported for 30 wt% β-MnO_2 nanorod loaded paraffin wax composite at 2.75 mm thickness [26]. The temperature response of the microwave attenuation of β-MnO_2 nanorod is explained in the literature [27]. According to this, the β-MnO_2 nanorod possesses high dielectric loss and microwave absorption at high temperature (~737 K) [25]. Moreover, the dielectric property of β-MnO_2 nanorod also can be tuned by preparing core shell structure such as β-MnO_2/SiO_2 [26]. According to the literature [28], few nanometer coating of SiO_2 (~5 nm) over β-MnO_2 nanorods results in high microwave absorption at high temperature [28].

Polyvinylbutyral (PVB) is a novel polymer that has recently drawn significant attention for encapsulation, especially in organic electronics, because of its unique moisture resistivity, dielectric properties, good mechanical properties as well as good adhesion to particles [3,29,30]. PVB has excellent adhesive properties with many materials such as glass, metals, plastics and wood, good light stability and moisture insensitivity [29,31]. The α-MnO_2 has better microwave absorption property as compared to other forms (β-MnO_2 and γ-MnO_2) [32]. As microwave absorption is morphology dependent, the objective of this work is the preparation and determination of microwave absorption of various morphologies of α-MnO_2 nanostructures loaded PVB nanocomposites.

2. Experimental

2.1. Materials

PVB was purchased from Synpol products Private Limited, India (SYNPOL B-30, density 1.05, Molecular weight 30,000 Da). Potassium permanganate ($KMnO_4$), manganese sulphate monohydrate ($MnSO_4.H_2O$), ethanol and HCl in analytical grade were purchased from the Polysales Private Limited and used without further purification.

2.2. Synthesis of MnO_2 nanorods

40 mM $KMnO_4$ and 60 mM $MnSO_4 \cdot H_2O$ were dissolved in 170 ml DI water at 25 °C and magnetically stirred for 30 min to form a homogeneous solution. The solution was then transferred into an oil bath preset at 80 °C and the reaction was allowed to proceed for 24 h. After the reaction was completed, the solution was allowed to cool down naturally to room temperature. The solid products obtained were centrifuged and washed several times with DI water and with absolute ethanol and finally dried at 100 ± 3 °C for 8 h. The black powdered particles obtained were then finely grinded.

The following reaction takes place during the synthesis:

$$3\ MnSO_4 \cdot H_2O + 2\ MnO_4^- \rightarrow 3\ SO_4^{2-} + 4\ H^+ + 5\ MnO_2(s) + H_2O(1)$$

The mechanism of formation of MnO_2 nanorods has been discussed in the literature [4].

2.3. Synthesis of MnO_2 nanospheres

The synthesis of MnO_2 nanospheres was carried out according to the literature [33]. In a typical synthesis, 10 ml of 6 M HCl was added drop wise to 50 ml of 0.1 M $KMnO_4$ solution prepared in a 200 ml beaker. Further, the solution was kept for stirring at room temperature for 2 h. After 2 h, the obtained solids were centrifuged and washed several times with DI water, and then dried under vacuum for 24 h.

According to the literature [33], the following are possible sources of MnO_2 in this synthesis:

$$2\ KMnO_4 + 8\ HCl \rightarrow 2\ KCl + 2\ MnO_2 + 4H_2O + 3\ Cl_2 \quad (2)$$

$$4\ KMnO_4 + 18\ HCl + 2\ e^- \rightarrow 4\ KCl + 2\ HMnO_4^- + 2\ MnCl_2 + 8H_2O + 5\ Cl_2 \quad (3)$$

$$MnCl_2 + 4\ HCl + 2\ O_2 \rightarrow MnO_2 + 2H_2O + 3\ Cl_2 \quad (4)$$

2.4. Preparation of PVB-MnO_2 nanocomposites

The PVB-MnO_2 nanocomposites were prepared by a solution processing technique. The PVB was dissolved in 10 ml ethanol. To this solution, 5 wt % of as synthesized MnO_2 nanospheres/nanorods were added very slowly and stirred for 1 h. After that, 3 ml DI water was added drop wise to this solution and the hydrophobic gel obtained was washed several times with DI water and poured into rectangular copper sample holders and kept for open air drying for 48 h.

2.5. Material characterization

The morphology induced crystal structures were studied by using X-Ray diffractrometer (Rigaku) in the scattering range of 2θ of 10–80°. The synthesized MnO_2 samples (nanorods and nanospheres) and their composites were coated over carbon tape and sputter coated with gold to examine the surface morphology by using high-resolution scanning electron microscope (FESEM, Carl Zeiss). The dielectric study of the prepared polymer nanocomposites was carried out in the X-band (8.2–12.4 GHz) and Ku-band (12.4–18 GHz) frequency range by using a vector network analyzer (VNA, Agilent NS201) through waveguide method [34]. The dielectrics of MnO_2 nanorods/nanospheres were measured by cavity perturbation method [35]. For that, the powder samples (MnO_2 nanorods/nanospheres) were inserted in a small borosilicate capillary tube and measurements were carried out at 8.2 GHz.

2.6. Microwave absorbing property

The complex *S*-parameters (S_{21}, S_{12}, S_{11}, S_{22}) were determined for PVB, PVB-MnO_2 nanorod and PVB-MnO_2 nanosphere composites

by the waveguide method, in both X-band and Ku-band. The standard two port, thru-reflect-line (TRL) calibration of VNA was performed and the complex permittivity ($\varepsilon_r = \varepsilon' - i\varepsilon''$) and permeability ($\mu_r = \mu' - i\mu''$), values were calculated by using Nicolson-Ross-Weir (NRW) algorithm [3,34] from the obtained *S*-parameters. The real part of complex permittivity (ε') is associated with the amount of polarization that corresponds to the storage ability of the electric energy from an electric field in the material. The imaginary part (ε'') corresponds to the amount of energy dissipated in the material due to an external electric field [12].

The microwave absorption properties of the as prepared composites were calculated in terms of reflection loss (RL) [36,37,49]. The optimum RL value of −10 dB is required for practical applications that corresponds to 90% absorption [36,49]. The attenuation of the incident energy on the surface of a microwave absorbing material backed with a perfect conductor is mainly due to reflection and transmission [38]. Thus, for the present system, transmission line model is applicable where backed conductor acts as the load of the transmission line. Hence, RL (dB) of the absorbing material having metal backed can be expressed as [38,39].

$$RL = 20\, log\left|\frac{Z_{in} - Z_0}{Z_{in} + Z_0}\right| \tag{5}$$

In eqn. (5), Z_0 and Z_{in} are the intrinsic impedance of free space and the material given by

$$Z_{in} = \eta_0 tanh\left(j\frac{2\pi d}{\lambda_0}\sqrt{\mu_r\varepsilon_r}\right) = Z_0\sqrt{\frac{\mu_r}{\varepsilon_r}}tanh\left(j\frac{2\pi d}{\lambda_0}\sqrt{\mu_r\varepsilon_r}\right) \tag{6}$$

λ_0 is the wavelength of the incident wave in free space while ε_r and μ_r represent the complex permittivity and permeability of the material.

3. Results and discussion

Fig. 1 shows the XRD patterns of as synthesized MnO_2 nanorod and MnO_2 nanosphere. The diffraction peaks of as synthesized MnO_2 nanorod can be indexed to the tetragonal α-MnO_2 phase [39]. In addition, no impurities were detected and the peaks in the XRD pattern confirm the presence of pure phase of α-MnO_2. Both MnO_2 nanorod and MnO_2 nanosphere samples exhibits almost similar diffraction peaks.

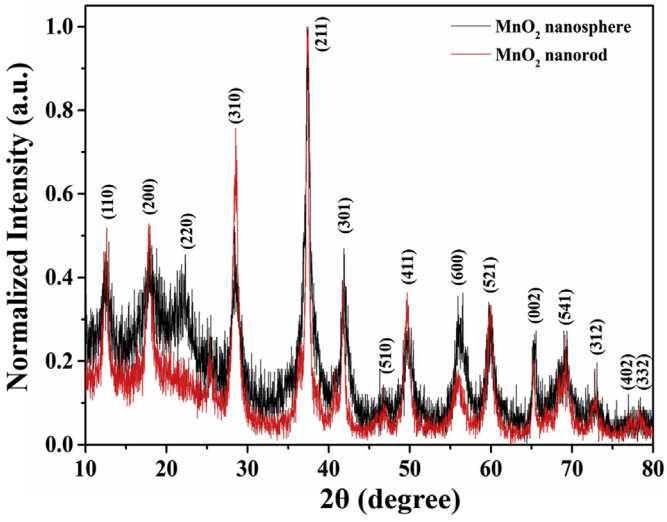

Fig. 1. XRD patterns of MnO_2 nanorods and MnO_2 nanospheres.

The surface morphologies of as synthesized MnO_2 nanosphere and MnO_2 nanorod are shown in Fig. 2(a) and (b, c), respectively. The observed morphology shows that the MnO_2 nanospheres is composed of worm like fibres aggregating on the surface of nanospheres. The diameter of MnO_2 nanosphere was obtained as ~162 ± 5 nm. Fig. 2(b, c) shows the surface morphology of the synthesized MnO_2 nanorods and the diameter and the length were ~40 ± 3 nm and ~1 ± 0.1 μm respectively. The cross sectional FESEM images of PVB-MnO_2 nanocomposites are shown in Fig. 3. From Fig. 3(a–c), it was observed that the MnO_2 nanoparticles (nanorods and nanospheres) are being grafted in the PVB matrix. Fig. 3 (d) shows the Mn elemental mapping of PVB-MnO_2 nanorod composite. The dense elemental mapping of Mn indicates the presence of MnO_2 nanorods throughout the PVB nanocomposite.

Fig. 4(a) and (b) shows the variation of ε' and ε'' of PVB-MnO_2 nanorod composite and PVB-MnO_2 nanosphere composites in the X-band. The ε' was found to be ~2.5, whilst ε'' was found to be ~0.1 for PVB. The ε' and ε'' was found to be 4 and 0.5 respectively for PVB-MnO_2 nanosphere composite. In the case of PVB-MnO_2 nanorod composite, the ε' increased up to ~12.5 and ε'' increased up to ~6.5. The values of ε' and ε'' of the MnO_2 nanorods were found to be ~11.3 and ~5.7 respectively (at 8.2 GHz). Similarly, the obtained ε' and ε'' values of MnO_2 nanosphere were ~2.3 and ~0.3 respectively. This shows that the addition of PVB enhances the dielectric properties of the MnO_2 nanorods/nanospheres, which is intrinsically important for microwave absorption. Fig. 5(a) and (b) shows the variation of ε' and ε'' of the as prepared PVB-MnO_2 nanocomposites in the Ku-band. The ε' of PVB for Ku-band was found to be ~2.3. For PVB-MnO_2 nanosphere composite, it increased up to ~3.5 and for PVB-MnO_2 nanorod composite it was found to be ~9 and decreases with frequency (~6 at 18 GHz). The ε'' of PVB was found to be ~0.1 and the ε'' of PVB-MnO_2 nanosphere composite was found to be ~0.7. The ε'' of PVB-MnO_2 nanorod composite was found to be ~8 and decreases to ~7.5 for Ku-band.

As anisotropic nanoparticles (especially 1D) have higher surface area and low percolation threshold, it can improve the dielectric permittivity more efficiently in the polymer matrix as compared to spherical structure [40]. Thus, the presence of MnO_2 nanorods in the PVB matrix increases the heterogeneity of the composite which effects on interfacial polarization as compared to MnO_2 nanospheres. The dielectric loss in polymer nanocomposites takes place due to the dc conductivity as well as ac conductivity or ion jump, dipole relaxation and interfacial polarization [41–43]. That is why a noticeable decrease in ε' and ε'' of PVB-MnO_2 nanorod composite with increase in frequency was observed for both X-band and Ku-band. According to Debye theory, the ε'' is due to the both polarization and electrical conductivity [44]. For the present case, the polarization refers to the interface and dipole polarization as electronic and ionic polarization usually takes place in the ultraviolet or infrared frequency regions [45]. In case of PVB-MnO_2 nanosphere composite, the ε'' value lies 0.5 to 0.7, i.e., difference of ε'' ($\Delta\varepsilon''$) *is* 0.2. On the other hand, the obtained $\Delta\varepsilon''$ value of PVB-MnO_2 nanorods is ~1. As higher $\Delta\varepsilon''$ value corresponds to stronger interfacial polarization, therefore, morphology also affects interfacial polarization of PVB-MnO_2 nanocomposites and in the case of PVB-MnO_2 nanorod, the interfacial polarization is intrinsically dominant [45].

The ratio of imaginary part (ε'') to real part (ε') of the complex permittivity is represented by the term tan δ which is also known as dielectric loss tangent, i.e., $tan\,\delta = \varepsilon''/\varepsilon'$ [46,47]. In case of non-magnetic materials, the dielectric loss leads to weak EM attenuation and hence tan δ is an important factor [46,47]. Fig. 6(a) and (b) shows the dielectric loss tangent ($tan\,\delta$) for PVB, PVB-MnO_2 nanosphere and PVB-MnO_2 nanorod composites for both X-band and Ku-band, respectively. For all the composites, the $tan\,\delta$ value

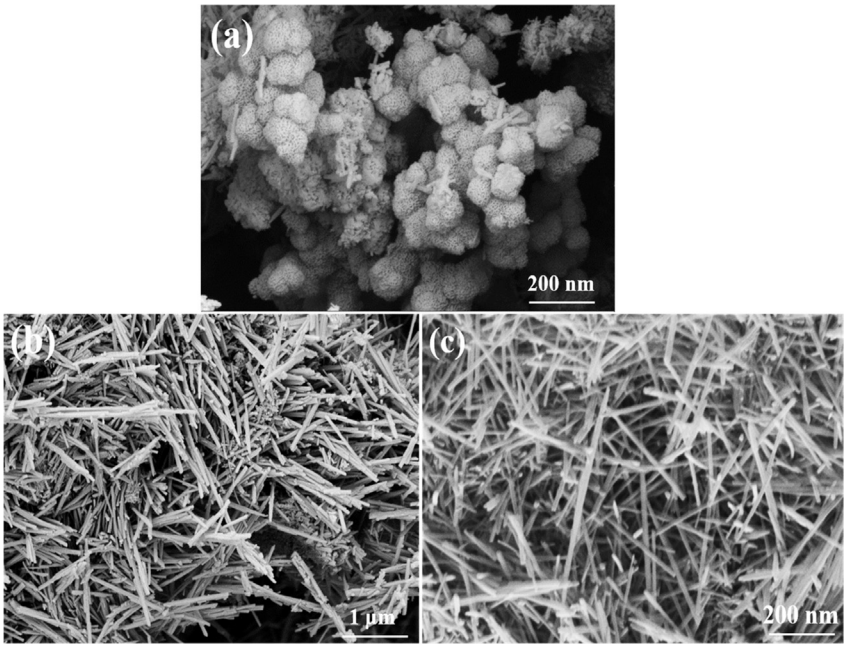

Fig. 2. FESEM images of (a) MnO_2 nanosphere and (b, c) MnO_2 nanorod.

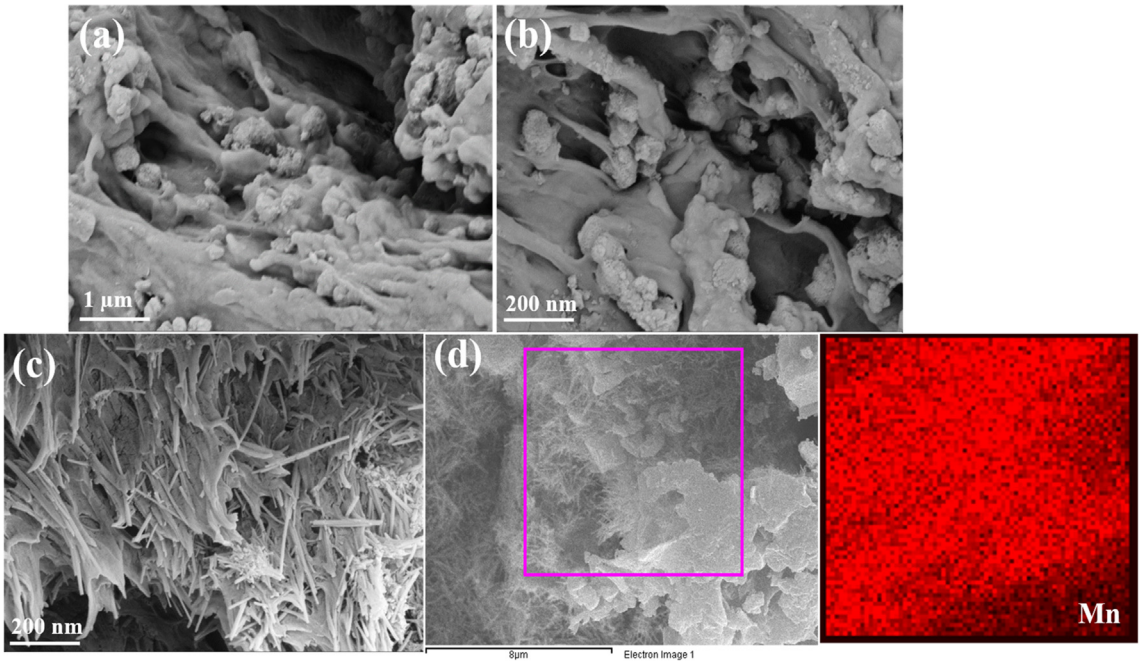

Fig. 3. Cross sectional FESEM images of (a, b) PVB-MnO_2 nanosphere composite, (c, d) PVB-MnO_2 nanorod composites and Mn elemental mapping respectively.

seems to be increasing with increase in the frequency for both X-band and Ku-band, and this increase was found to be very small for both PVB and PVB-MnO_2 nanosphere composite compared to that of PVB-MnO_2 nanorod composite. For X-band, the *tan δ* of PVB-MnO_2 nanorod composite reaches ~0.55 at 12.4 GHz and for Ku-band, it reaches up to ~1.3 at 18 GHz.

The RL of the composites was calculated using Eqn. (5). Fig. 7(a) and (b) shows the obtained RL at different thicknesses of the PVB-MnO_2 nanosphere and PVB-MnO_2 nanorod composite for the X-band and Ku-band, respectively. As shown in the Fig. 7(a) and (b), the minimum RL value of PVB-MnO_2 nanorod and PVB-MnO_2 nanosphere composites was found to be −5 dB to −39 dB and −0.25 dB to − 13 dB respectively. It is evident from Fig. 7(a) and (b) that PVB-MnO_2 nanorods have lower RL values compared to that of PVB-MnO_2 nanosphere for all thicknesses in X-band.

It was observed that the peak values of RL shift to a lower frequency with increasing absorber thickness (Figs. 7 and 8). This is due to the quarter-wavelength cancellation model [43]. When a microwave of particular frequency incidents on an absorber, its wavelength λ_{in} can be expressed as [48],

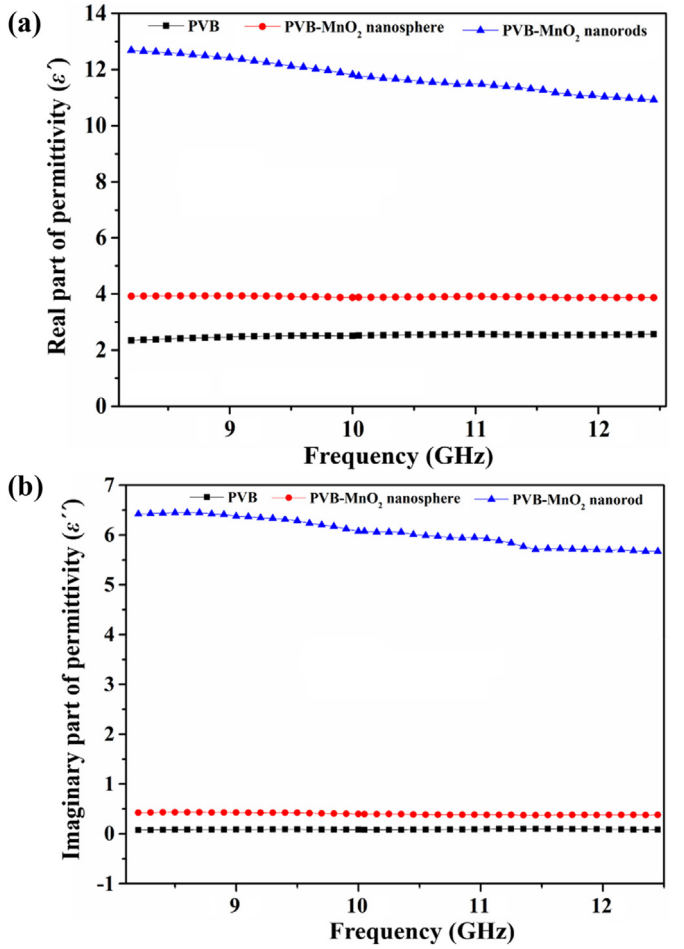

Fig. 4. Variation of (a) real (ε') and (b) imaginary (ε'') part of relative complex permittivity of PVB, PVB-MnO_2 nanosphere and PVB-MnO_2 nanorod composites for X-band.

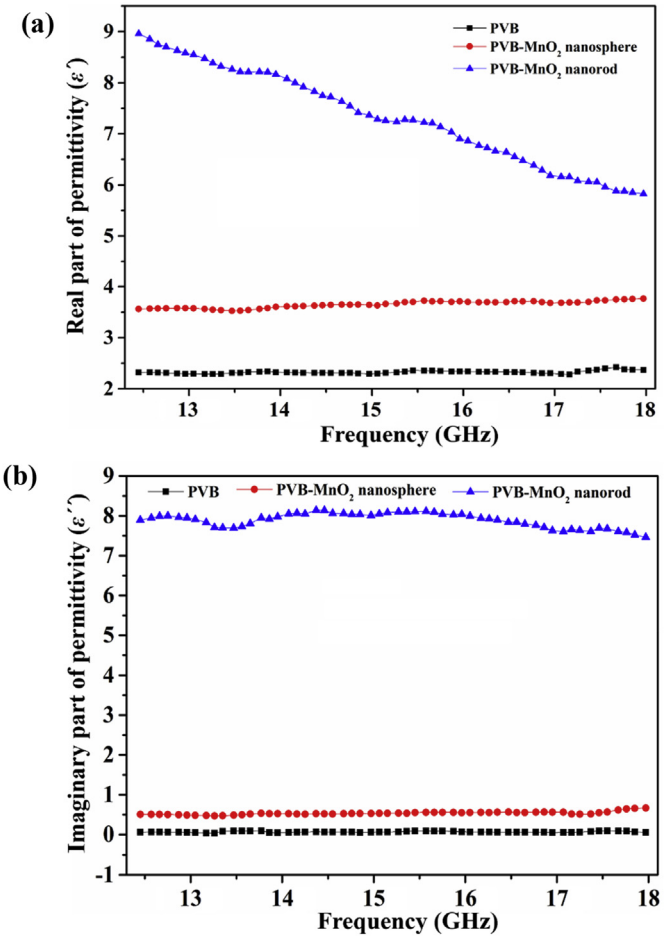

Fig. 5. Variation of (a) real (ε') and (b) imaginary (ε'') part of complex relative permittivity of PVB, PVB-MnO_2 nanosphere and PVB-MnO_2 nanorod composites for Ku-band.

$$\lambda_{in} = \frac{\lambda_{air}}{\sqrt{|\mu_r||\varepsilon_r|}} \tag{7}$$

If the absorber thickness d equals to $\frac{1}{4\lambda_{in}}$, the reflected wave and incident wave will cancel each other out in the interface between the air and the absorber. The relationship between the absorber thickness *(d)* and the particular frequency *(f)* can be expressed as the following equation [48],

$$d = \frac{nc}{4f\sqrt{|\mu_r||\varepsilon_r|}} \tag{8}$$

Where, $n = 1, 3, 5 \ldots$ and c is the speed of light. Thus, in terms of RL value, Eqn. (8) suggests, f will shift to lower frequency with increasing absorber thickness.

Fig. 8 shows the comparison of RL values of PVB, PVB-MnO_2 nanorod and PVB-MnO_2 nanosphere composites at the same thickness (2 mm). For both X-band and Ku-band, PVB-MnO_2 nanorod composites exhibit the lowest RL value with high bandwidth (less than −10 dB) compared to that of PVB-MnO_2 nanosphere composite. The bandwidth can be adjusted by adjusting the absorber thickness [49] and in the case of PVB-MnO_2 nanorod composite, the largest bandwidth (RL ≤ -10 dB) was achieved for the optimal thickness of 2 mm (8.2–18 GHz). In case of PVB-MnO_2 nanosphere, the minimum RL value was −8 dB for the same thickness. This indicates that the morphology also helps to achieve wide band width (RL ≤ -10 dB) with minimum thickness. The microwave absorption efficiency, R_E can be expressed as, $R_E = \frac{\Delta S}{d}$, where, $\Delta S = \int RL\, df_{RL \leq -10\ dB}$ [49]. The microwave absorption efficiency of PVB-MnO_2 nanorod composite can be expected to be very high as compared to PVB-MnO_2 nanosphere composite (no specific RL bandwidth was observed for PVB-MnO_2 nanosphere composite till 3 mm). A comparison of RL value of PVB-MnO_2 nanorod composite with recently reported composites is shown in Table 1 and it shows that the present polymer nanocomposite is much superior in terms of low filler content and thickness.

The electromagnetic wave propagates inside a material through its time average power and it travels exponentially decreasing the magnitude and by changing phase [3]. The propagation factor (γ_s) of the electromagnetic wave inside a material is given by,

$$\gamma_s = \sqrt{j\omega\mu\acute{\sigma}} \tag{9}$$

In Eqn. (9), ω is the angular frequency, μ' is the permeability and σ is the electrical conductivity.

The real part of γ_s is known as EM attenuation constant *(α)*, which plays an important role in the microwave absorption of the materials. It is associated with the interfacial polarization, space charge polarization and relaxation phenomenon, as it depends on the morphology and dispersion of the fillers in the matrix [2]. The morphology affects the EM impedance matching degree (Δ) which

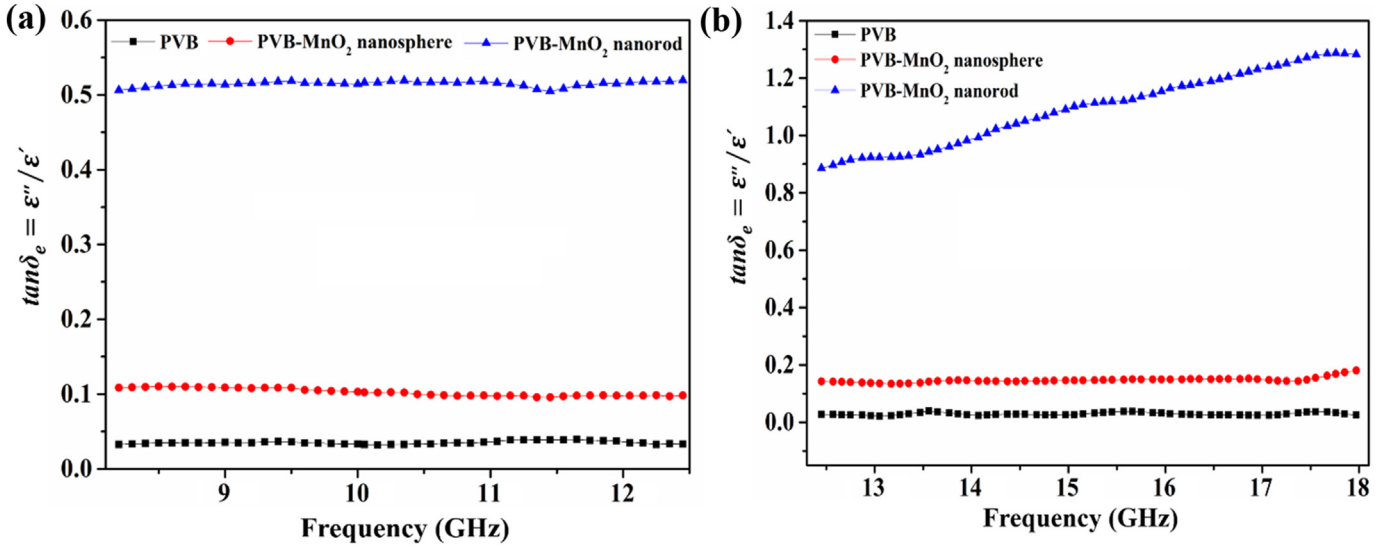

Fig. 6. Dielectric loss tangent of PVB, PVB-MnO_2 nanosphere and PVB-MnO_2 nanorod for (a) X-band and (b) Ku-band.

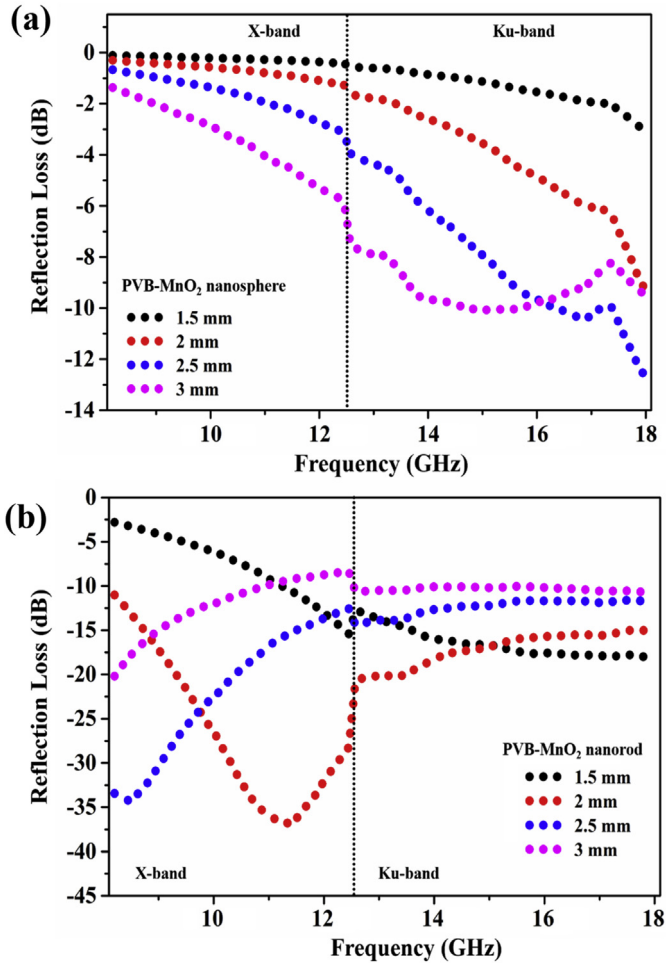

Fig. 7. Variation of reflection loss (RL, dB) of (a) PVB-MnO_2 nanosphere composite and (b) PVB-MnO_2 nanorod composite.

can be expressed as [51],

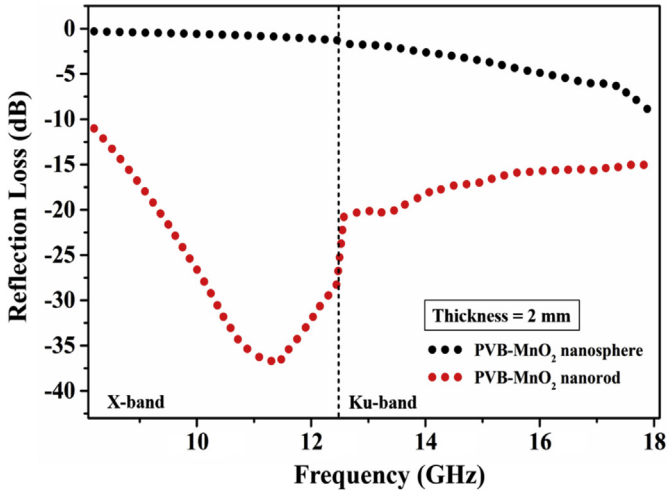

Fig. 8. Comparison of RL of PVB-MnO_2 nanosphere and PVB-MnO_2 nanorod composite.

$$\Delta = \left| sinh^2(Kfd) - M \right| \tag{10}$$

Where, K and M depends on the relative complex permittivity and permeability as follows [51],

$$K = \frac{4\pi\sqrt{\mu\acute{\varepsilon}''}}{c} \; \frac{\sin[(\delta_e + \delta_m)/2]}{cos\delta_e \, cos\delta_m} \tag{11}$$

$$M = [4\mu\acute{c}os\delta_e\varepsilon\acute{c}os\delta_m].\left[(\mu\acute{c}os\delta_e - \varepsilon\acute{c}os\delta_m)^2 + \left(tan\frac{\delta_m - \delta_e}{2}\right)^2 (\mu\acute{c}os\delta_e + \varepsilon\acute{c}os\delta_m)^2\right]^{-1} \tag{12}$$

The composite materials are non-magnetic, therefore $\mu' = 1$. The variation of EM impedance matching degree (Δ) of PVB-MnO_2 nanocomposites (thickness 1.5 mm) is shown Fig. 9. The change of Δ value with frequency suggests better microwave absorption property of the material. For an ideal microwave absorber, Δ value

Table 1
Optimum RL (dB) of various reported materials with present work.

Material	Frequency (GHz)	Reflection loss (dB)	Filler content/Ratio	Thickness (mm)	Reference
PVB/Fe-MnO_2	14.7	−15.7	10 wt%	2	[38]
Polydopamine@α-MnO_2	9.68	−21. 8	5:1	3	[15]
$MnFe_2O_4$/PVDF	9.5	−5	10 wt%	3	[12]
RGO/$MnFe_2O_4$/PVDF	9.2	−29	5 wt%	3	[12]
Mn_3O_4/Paraffin wax	3.1	−27.1	50 wt%	6	[24]
Paraffin/β-MnO_2 micron cube	15	−13.3	30 wt%	2	[50]
Paraffin/β-MnO_2 nanorod	5	−8	1:1	2.5	[23]
Paraffin/Fe/β-MnO_2 nanorod	15	−10	1:1	2.5	[23]
PVB/α-MnO_2 nanorod	11.5	- 37	5 wt%	2	Present work

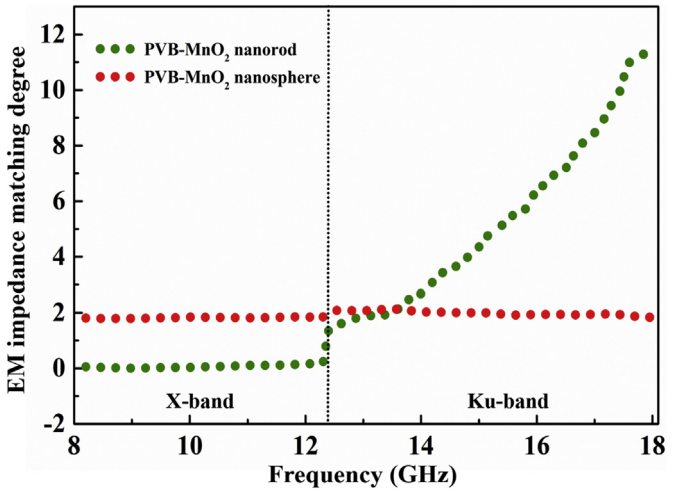

Fig. 9. Variation of EM impedance matching degree (Δ) of PVB-MnO_2 nanorod/nanosphere composites (thickness 1.5 mm).

must gradually approach to zero [51]. As in the case of PVB-MnO_2 nanorod composite, the dielectric dissipation is higher (especially in X-band) as compared to PVB-MnO_2 nanosphere composite. Therefore, Δ value of PVB-MnO_2 nanorod composite gradually decreases from high frequency to low frequency. On the other hand, the change of Δ value is negligible for PVB-MnO_2 nanosphere compared to PVB-MnO_2 nanorod. In the X-band, the obtained Δ value approaches zero for PVB-MnO_2 nanorods, whilst Δ is ~2 for PVB-MnO_2 nanosphere composite. This suggests that the MnO_2 nanorod loaded PVB possess high microwave absorption property in the X-band.

As discussed above, the microwave absorption property of a dielectric material is intrinsically controlled by EM attenuation constant (α) along with impedance matching [3,5]. The equation of α is,

$$\alpha = \frac{\sqrt{2}\pi f}{c} \times \left[\left(\mu'' \varepsilon'' - \mu' \varepsilon' \right) + \left\{ \left(\mu'' \varepsilon'' - \mu' \varepsilon' \right)^2 + \left(\mu' \varepsilon'' + \mu'' \varepsilon' \right)^2 \right\}^{\frac{1}{2}} \right]^{\frac{1}{2}} \quad (13)$$

Where, f and c represents the frequency and velocity of the light respectively.

Fig. 10(a) and (b) shows the frequency dependant variation of α value of PVB, PVB-MnO_2 nanosphere and PVB-MnO_2 nanorod composites in X-band and Ku-band respectively. The α value obtained for PVB was ~5 for X-band and Ku-band. The α value of PVB-MnO_2 nanosphere composite was found to be ~25. On the other hand, α value of PVB-MnO_2 nanorod composite increases from 150 to 210 for X-band and reaches ~500 in the Ku-band. Thus, the significant enhancement of EM attenuation constant of PVB-MnO_2 nanorod composite in both X-band and Ku-band in comparison with that of PVB and PVB-MnO_2 nanosphere composites indicates that, the improvement of microwave absorption property of PVB matrix with MnO_2 nanorod is very high compared to that of MnO_2 nanosphere. In addition to this, the microwave antenna mechanism is also applicable for dielectric nanorods. According to this, the MnO_2 nanorods also can act as an antenna for incident electromagnetic energy and transmits through micro current which

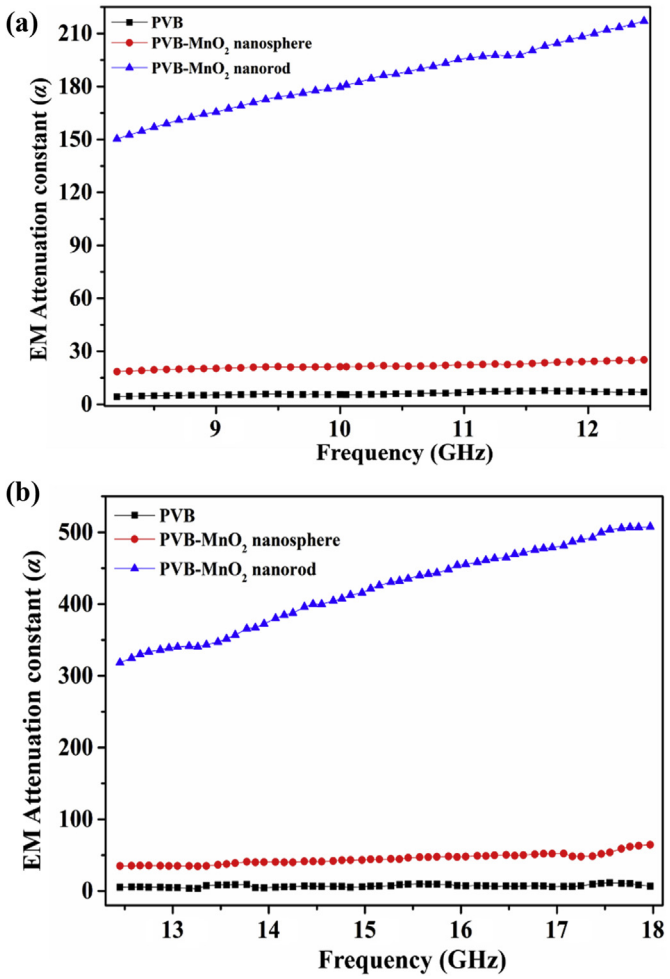

Fig. 10. Variation of EM attenuation constant (α) of PVB, PVB-MnO_2 nanosphere, PVB-MnO_2 nanorod composite in the (a) X-band and (b) Ku-band respectively.

dissipates in the materials [18,20]. Moreover, if the effective media theory is considered, then it also indicates that the enhancement of effective permittivity depends on morphology. The MnO_2 nanorod can be treated as a uniaxial dielectric [22]. Thus the presence of MnO_2 nanorods in the PVB indicates more effective permittivity, as compared to MnO_2 nanospheres.

Apart from above discussion, high microwave absorption property of PVB-MnO_2 nanorod composite also can be understand in terms of loss factor (LF) [52]. The LF is expressed as,

$$LF(\%) = 100 \times \left(1 - |RC|^2 - |TC|^2\right) \quad (14)$$

RC is the reflection co-efficient and TC is the transmission co-efficient in linear form.

The variation of LF of PVB-MnO_2 nanosphere composite and PVB-MnO_2 nanorod composite is shown in the Fig. 11. It was observed that the LF of PVB-MnO_2 nanosphere composite is ~62% in the frequency range 8.2–18 GHz. On the other hand, the LF of PVB-MnO_2 nanorod composite increases with frequency and reached maximum 84% at 18 GHz. Thus it indicates the excellent microwave absorption property of PVB-MnO_2 nanorod composite.

4. Conclusions

The morphology controlled microwave absorption properties of PVB-MnO_2 nanocomposites were studied. For filler loading of 5 wt %, high dielectric nature of PVB-MnO_2 nanorod composite was observed as compared to PVB-MnO_2 nanosphere composite. MnO_2 nanorod loaded PVB nanocomposite is found more efficient for microwave absorption as compared to MnO_2 nanosphere. The minimum RL value of −37 dB of PVB-MnO_2 nanorod composite was obtained with large band width in X-band for the thickness of 2 mm. The factors such as effective permittivity, degree of EM impedance matching, antenna mechanism, and dielectric dissipation was found to depend on the morphology of PVB-MnO_2 nanocomposites. The enhancement of EM attenuation constant (α) and dielectric loss is also high for PVB-MnO_2 nanorod composite. Moreover, the loss factor of PVB-MnO_2 nanorod composite is also very high (reached up to 84%) and thus it can be considered as a novel microwave absorbing coating material for various microwave based applications.

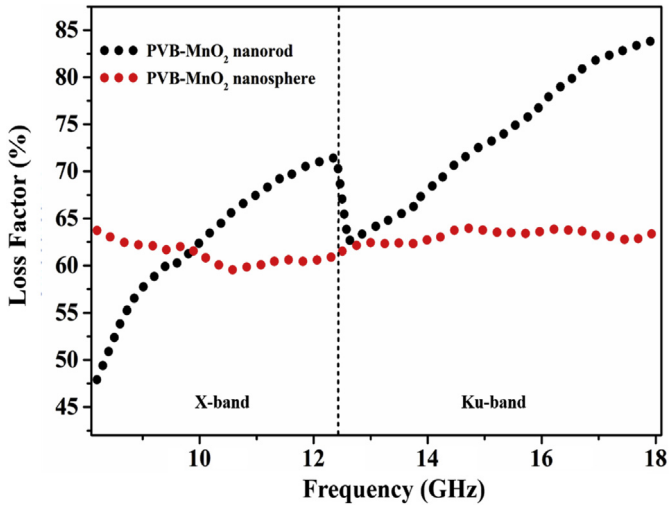

Fig. 11. Variation of loss factor (LF %) of PVB-MnO_2 nanosphere and PVB-MnO_2 nanorod composite with frequency.

Acknowledgements

The authors gratefully acknowledge the Department of Science and Technology (DST), India for financial support (SB/S3/ME/51/2012) and IISc advanced characterization centre and CeNSE for technical support. Giridhar Madras acknowledges DST for the J.C. Bose fellowship.

References

[1] Zhao B, Fan B, Shao G, Zhao W, Zhang R. Facile Synthesis of novel hetero-structure based on SnO_2 nanorods grown on submicron Ni walnut with tunable electromagnetic wave absorption capabilities. ACS Appl Mater Interfaces 2015;7:18815–23.
[2] Shan L, Chen X, Tian X, Chen J, Zhou Z, Jiang M, et al. Fabrication of polypyrrole/nano-exfoliated graphite composites by in situ intercalation polymerization and their microwave absorption properties. Compos Part B Eng 2015;73:181–7.
[3] Bora PJ, Mallik N, Ramamurthy PC, Kishore, Madras G. Poly(vinyl butyral)-polyaniline-magnetically functionalized fly ash cenosphere composite film for electromagnetic interference shielding. Compos Part B Eng 2016;106:224–33.
[4] Guan H, Xie J, Chen G, Wang Y. Facile synthesis of α-MnO_2 nanorods at low temperature and their microwave absorption properties. Mater Chem Phys 2014;143:1061–8.
[5] Zhao B, Fan B, Xu Y, Shao G, Wang X, Zhao W, et al. Preparation of honeycomb SnO_2 foams and configuration-dependent microwave absorption features. ACS Appl Mater Interfaces 2015;7:26217–25.
[6] Tang H, Jian X, Wu B, Liu S, Jiang Z, Chen X, et al. Fe_3C/helical carbon nanotube hybrid: facile synthesis and spin-induced enhancement in microwave-absorbing properties. Compos Part B Eng 2016;107:51–8.
[7] Qin F, Brosseau C. A review and analysis of microwave absorption in polymer composites filled with carbonaceous particles. J Appl Phys 2012;111:061301.
[8] Che RC, Peng L-M, Duan XF, Chen Q, Liang XL. Microwave absorption enhancement and complex permittivity and permeability of Fe encapsulated within carbon nanotubes. Adv Mater 2004;16:401–5.
[9] Wen B, Cao M, Lu M, Cao W, Shi H, Liu J, et al. Reduced graphene oxides: light-weight and high-efficiency electromagnetic interference shielding at elevated temperatures. Adv Mater 2014;26:3484–9.
[10] Zou C, Yao Y, Wei N, Gong Y, Fu W, Wang M, et al. Electromagnetic wave absorption properties of mesoporous Fe_3O_4/C nanocomposites. Compos Part B Eng 2015;77:209–14.
[11] Bibi M, Abbas SM, Ahmad N, Muhammad B, Iqbal Z, Rana UA, et al. Microwaves absorbing characteristics of metal ferrite/multiwall carbon nanotubes nanocomposites in X-band. Compos Part B Eng 2017;114:139–48.
[12] Zhang X-J, Wang G-S, Cao W-Q, Wei Y-Z, Liang J-F, Guo L, et al. Enhanced microwave absorption property of reduced graphene oxide (RGO)-$MnFe_2O_4$ nanocomposites and polyvinylidene fluoride. ACS Appl Mater Interfaces 2014;6:7471–8.
[13] Tian C, Du Y, Xu P, Qiang R, Wang Y, Ding D, et al. Constructing uniform core–shell PPy@PANI composites with tunable shell thickness toward enhancement in microwave absorption. ACS Appl Mater Interfaces 2015;7:20090–9.
[14] Bora PJ, Lakhani G, Ramamurthy PC, Madras G. Outstanding electromagnetic interference shielding effectiveness of polyvinylbutyral–polyaniline nanocomposite film. RSC Adv 2016;6:79058–65.
[15] She W, Bi H, Wen Z, Liu Q, Zhao X, Zhang J, et al. Tunable microwave absorption frequency by aspect ratio of hollow polydopamine@α-MnO_2 microspindles studied by electron holography. ACS Appl Mater Interfaces 2016;8:9782–9.
[16] Yan D, Cheng S, Zhuo RF, Chen JT, Feng JJ, Feng HT, et al. Nanoparticles and 3D sponge-like porous networks of manganese oxides and their microwave absorption properties. Nanotechnology 2009;20:105706.
[17] Yang H-J, Cao W-Q, Zhang D-Q, Su T-J, Shi H-L, Wang W-Z, et al. NiO hierarchical nanorings on SiC: enhancing relaxation to tune microwave absorption at elevated temperature. ACS Appl Mater Interfaces 2015;7:7073–7.
[18] Zhao B, Shao G, Fan B, Guo W, Xie Y, Zhang R. Facile synthesis of Ni/ZnO composite: morphology control and microwave absorption properties. J Magn Magn Mater 2015;382:78–83.
[19] Zhao B, Shao G, Fan B, Xie Y, Sun B, Zhang R. Preparation and microwave absorption of porous hollow ZnO by CO_2 soft-template. Adv Powder Technol 2014;25:1761–6.
[20] Zhuo RF, Qiao L, Feng HT, Chen JT, Yan D, Wu ZG, et al. Microwave absorption properties and the isotropic antenna mechanism of ZnO nanotrees. J Appl Phys 2008;104:094101.
[21] Ballav N. High-conducting polyaniline via oxidative polymerization of aniline by MnO_2, PbO_2 and NH_4VO_3. Mater Lett 2004;58:3257–60.
[22] Bora PJ, Vinoy KJ, Ramamurthy PC, Madras G. Electromagnetic interference shielding efficiency of MnO_2 nanorod doped polyaniline film. Mater Res Express 2017;4:025013.
[23] Wang Y, Han B, Chen N, Deng D, Guan H, Wang Y. Enhanced microwave absorption properties of MnO_2 hollow microspheres consisted of MnO_2

nanoribbons synthesized by a facile hydrothermal method. J Alloys Compd 2016;676:224–30.
[24] Zhou M, Zhang X, Wei J, Zhao S, Wang L, Feng B. Morphology-controlled synthesis and novel microwave absorption properties of hollow urchinlike α-MnO_2 nanostructures. J Phys Chem C 2011;115:1398–402.
[25] Lv H, Ji G, Liang X, Zhang H, Du Y. A novel rod-like MnO_2@Fe loading on graphene giving excellent electromagnetic absorption properties. J Mater Chem C 2015;3:5056–64.
[26] Song W-L, Cao M-S, Qiao B-B, Hou Z-L, Lu M-M, Wang C-Y, et al. Nano-scale and micron-scale manganese dioxide vs corresponding paraffin composites for electromagnetic interference shielding and microwave absorption. Mater Res Bull 2014;51:277–86.
[27] Shi X-L, Cao M-S, Fang X-Y, Yuan J, Kang Y-Q, Song W-L. High-temperature dielectric properties and enhanced temperature-response attenuation of β-MnO_2 nanorods. Appl Phys Lett 2008;93:223112.
[28] Shi X, Cao M, Fang X. β-MnO_2/SiO_2 core–shell nanorods: synthesis and dielectric properties. J Nanosci Nanotechnol 2011;11:6953–8.
[29] Roy AS, Saravanan S, Kishore, Ramamurthy PC, Madras G. Dielectric impedance studies of poly(vinyl butyral)–cenosphere composite films. Polym Compos 2014;35:1636–43.
[30] Gupta S, Seethamraju S, Ramamurthy PC, Madras G. Polyvinylbutyral based hybrid organic/inorganic films as a moisture barrier material. Ind Eng Chem Res 2013;52:4383–94.
[31] Nakane K, Kurita T, Ogihara T, Ogata N. Properties of poly(vinyl butyral)/TiO_2 nanocomposites formed by sol–gel process. Compos Part B Eng 2004;35:219–22.
[32] Guan H, Chen G, Zhang S, Wang Y. Microwave absorption characteristics of manganese dioxide with different crystalline phase and nanostructures. Mater Chem Phys 2010;124:639–45.
[33] Dang T-D, Cheney MA, Qian S, Joo SW, Min B-K. A novel rapid one-step synthesis of manganese oxide nanoparticles at room temperature using poly(dimethylsiloxane). Ind Eng Chem Res 2013;52:2750–3.
[34] Chen LF, Ong CK, Neo CP, Varadan VV, Varadan VK. Microwave electronics: measurement and materials characterization. John Wiley & Sons; 2004.
[35] Yang RB, Tsay CY, Hung DS, Liang WF, Yao YD, Lin CK. Complex permittivity and permeability of iron-based composite absorbers measured by cavity perturbation method in X-band frequency range. J Appl Phys 2009;105:07A528.
[36] Zhao B, Zhao W, Shao G, Fan B, Zhang R. Corrosive synthesis and enhanced electromagnetic absorption properties of hollow porous Ni/SnO_2 hybrids. Dalton Trans 2015;44:15984–93.
[37] Zhao B, Shao G, Fan B, Zhao W, Xie Y, Zhang R. Synthesis of flower-like CuS hollow microspheres based on nanoflakes self-assembly and their microwave absorption properties. J Mater Chem A 2015;3:10345–52.
[38] Bora PJ, Porwal M, Vinoy KJ, Ramamurthy PC, Madras G. Influence of MnO_2 decorated Fe nano cauliflowers on microwave absorption and impedance matching of polyvinylbutyral (PVB) matrix. Mater Res Express 2016;3:095003.
[39] Sanchez-Botero L, Herrera AP, Hinestroza JP. Oriented growth of α-MnO_2 nanorods using natural extracts from grape stems and apple peels. Nanomaterials 2017;7:117.
[40] Zeraati AS, Arjmand M, Sundararaj U. Silver nanowire/MnO_2 nanowire hybrid polymer nanocomposites: materials with high dielectric permittivity and low dielectric loss. ACS Appl Mater Interfaces 2017;9:14328–36.
[41] Kasagi T, Tsutaoka T, Hatakeyama K. Electromagnetic properties of Permendur granular composite materials containing flaky particles. J Appl Phys 2014;116:153901.
[42] Liu J, Cao W-Q, Jin H-B, Yuan J, Zhang D-Q, Cao M-S. Enhanced permittivity and multi-region microwave absorption of nanoneedle-like ZnO in the X-band at elevated temperature. J Mater Chem C 2015;3:4670–7.
[43] Zhao B, Shao G, Fan B, Zhao W, Zhang S, Guan K, et al. In situ synthesis of novel urchin-like ZnS/Ni_3S_2@Ni composite with a core–shell structure for efficient electromagnetic absorption. J Mater Chem C 2015;3:10862–9.
[44] Lu M, Wang X, Cao W, Yuan J, Cao M. Carbon nanotube-CdS core–shell nanowires with tunable and high-efficiency microwave absorption at elevated temperature. Nanotechnology 2016;27:065702.
[45] Lv H, Guo Y, Wu G, Ji G, Zhao Y, Xu ZJ. Interface polarization strategy to solve electromagnetic wave interference issue. ACS Appl Mater Interfaces 2017;9:5660–8.
[46] Zhao B, Shao G, Fan B, Zhao W, Zhang R. Investigation of the electromagnetic absorption properties of Ni@TiO_2 and Ni@SiO_2 composite microspheres with core–shell structure. Phys Chem Chem Phys 2015;17:2531–9.
[47] Zhao B, Shao G, Fan B, Zhao W, Xie Y, Zhang R. Facile preparation and enhanced microwave absorption properties of core–shell composite spheres composited of Ni cores and TiO_2 shells. Phys Chem Chem Phys 2015;17:8802–10.
[48] Huang X, Zhang J, Lai M, Sang T. Preparation and microwave absorption mechanisms of the NiZn ferrite nanofibers. J Alloys Compd 2015;627:367–73.
[49] Zhao B, Guo X, Zhao W, Deng J, Shao G, Fan B, et al. Yolk–shell Ni@SnO_2 composites with a designable interspace to improve the electromagnetic wave absorption properties. ACS Appl Mater Interfaces 2016;8:28917–25.
[50] Duan Y, Pang H, Zhang Y, Chen J, Wang T. Morphology-controlled synthesis and microwave absorption properties of β-MnO_2 microncube with rectangular pyramid. Mater Charact 2016;112:206–12.
[51] Zhi M, Chen-Tao C, Qing-Fang L, Jian-Bo W. A new method to calculate the degree of electromagnetic impedance matching in one-layer microwave absorbers. Chin Phys Lett 2012;29:038401.
[52] Micheli D, Apollo C, Pastore R, Marchetti M. X-Band microwave characterization of carbon-based nanocomposite material, absorption capability comparison and RAS design simulation. Compos Sci Technol 2010;70:400–9.